Available online at www.sciencedirect.com
SCIENCE DIRECT
Journal of Sound and Vibration 293 (2006) 819–829
JOURNAL OF SOUND AND VIBRATION
www.elsevier.com/locate/jsvi

Simulations of roughness initiation and growth on railway rails

X. Sheng[a], D.J. Thompson[a,*], C.J.C. Jones[a], G. Xie[b], S.D. Iwnicki[b], P. Allen[b], S.S. Hsu[b]

[a]*ISVR, University of Southampton, Highfield, Southampton SO17 1BJ, UK*
[b]*Rail Technology Unit, Manchester Metropolitan University, Chester St, Manchester M5 1GD, UK*

Accepted 26 August 2005
Available online 23 January 2006

Abstract

A model for the prediction of the initiation and growth of roughness on the rail is presented. The vertical interaction between a train and the track is calculated as a time history for single or multiple wheels moving on periodically supported rails, using a wavenumber-based approach. This vertical dynamic wheel/rail force arises from the varying stiffness due to discrete supports (i.e. parametric excitation) and the roughness excitation on the railhead. The tangential contact problem between the wheel and rail is modelled using an unsteady two-dimensional approach and also using the three-dimensional contact model, FASTSIM. This enables the slip and stick regions in the contact patch to be identified from the input geometry and creepage between the wheel and rail. The long-term wear growth is then predicted by applying repeated passages of the vehicle wheelsets, as part of an iterative solution.

1. Introduction

It is well known that railway rolling noise is caused by the 'roughness' of the wheel and rail running surfaces, undulations with wavelengths between about 5 and 200 mm and amplitudes of the order of a micron [1]. This roughness induces vibrations of the wheel and track which, in turn, radiate noise. Models are available to predict the noise using physical parameters describing the wheel and track structures [2]. These models can be used in the design of low-noise vehicles and track. However, in these models the roughness is taken as an input which is normally assumed to be the same for all design variants considered. In practice the track or wheel design may affect the development of roughness. For example, it is found that a stiff rail pad is beneficial in reducing the track noise for a given roughness [3], yet it is believed that such a pad is more likely to lead to the formation of rail corrugation, e.g. Ref. [4]. A knowledge of how roughness grows is therefore vital for railway noise control at source. Considerable research has been carried out into the formation of rail corrugation. For rolling noise, however, not only periodic roughness (corrugation) but also broad-band roughness is of interest.

*Corresponding author. Tel.: +44 23 8059 2510; fax: +44 23 8059 3190.
E-mail address: djt@isvr.soton.ac.uk (D.J. Thompson).

0022-460X/$ - see front matter © 2006 Elsevier Ltd. All rights reserved.
doi:10.1016/j.jsv.2005.08.050

Grassie and Kalousek [5] classified rail corrugation into six groups according to their wavelength-fixing and damage mechanisms: (1) heavy haul corrugation (200–300 mm); (2) light rail corrugation (500–1500 mm); (3) booted sleepers-type corrugation (45–60 mm); (4) contact fatigue corrugation (150–450 mm); (5) rutting corrugation (150–450 and 50 mm for trams); (6) roaring rail (or short pitch) corrugation (25–80 mm).

Most of the recent work has been directed towards the modelling of short pitch corrugation. This is commonly associated with high-speed, main-line track with relatively light axle loads. It occurs predominantly on tangent track or in gentle curves in which there is no contact between the wheel flange and the gauge face of the rail. The main damage mechanism in its formation is believed to be the wear caused by the longitudinal (or lateral) slip between the wheel and rail at the slip zone of the contact patch. For train speeds between 20 and 70 m/s, short pitch corrugation gives rise to excitations predominantly in the frequency range of about 200–3000 Hz, coinciding with the frequency range of rolling noise. Therefore, in terms of railway rolling noise, short pitch corrugation is of greatest importance to the railway industry.

Müller [6], following the studies by Valdivia [7], Hempelmann [8] and Frederick [9], presented a linear, frequency-domain wheel-track model to predict instability and the formation of short pitch corrugation. A finite element model was used to model the dynamics of a single wheelset. The rail was described by an assembly of beams and plates and was assumed to be infinitely long and discretely supported by sleepers. Both the vertical and lateral track dynamics were included. A geometrical filter function due to the contact patch length was introduced which partly explains why corrugation wavelengths observed in practice vary little with train speeds.

To explore the wavelength-fixing mechanism for short pitch corrugation, Nielsen [10] conducted a study for a cylinder rolling on a sinusoidal rail profile without any influence of wheel/track dynamics. By extending the Hertzian contact theory for the normal contact stress and Carter's solution [11] for the tangential contact stress, the wear due to wheel/rail slip in the longitudinal direction was calculated. It was shown that sinusoidal irregularities increase preferentially in a particular wavelength range. In other words, the wavelength-fixing mechanism may partly exist within the contact mechanics.

Ilias [4] provides an approach in the time domain to the rail corrugation problem in which nonlinearity of the contact mechanics is taken into account as well as transient structural dynamics within the long-term wear process. A viscously damped track model is used. Starting with measured rail profiles, it is found from calculations that corrugations grow more quickly with stiffer railpads. In addition, a novel influence of the sleeper passing frequency is demonstrated, since for the chosen parameters and the very small initial roughness, parametric excitation from the discrete supports dominates the final profile.

The models mentioned above consider only a single wheel or wheelset, excluding effects from neighbouring wheels. Wu and Thompson [12] have demonstrated, using a frequency-domain approach, that the presence of multiple wheelsets in a bogie has a significant effect on the normal contact forces. They also presented an investigation of rail corrugation generation by combining the multiple wheel/rail vertical dynamics, a quasi-static two-dimensional contact mechanics model and wear process [13]. Igeland [14] presented a time-domain model that included two wheels and also showed the effects of reflections between the wheels. Nielsen used this model to investigate the development of broad-band roughness [15]. This time-domain approach has been extended recently to include a fuller contact model and used to predict corrugation generation [16].

Time-domain models require the infinitely long track to be truncated, which may cause wave reflections from the ends if the railpad is very soft [4]. A frequency-domain model can be more useful to give insight into the mechanisms involved in corrugation formation and roughness growth. However, in all the aforementioned frequency-domain models, the motion of the wheel along the rail is replaced by the motion of an 'irregularity strip' between the wheel and rail. Thus, the effect of the wheel speed cannot be taken into account. It has been shown in Refs. [17,18] that the wheel speed can have significant effects on wheel/rail interactions when the excitation frequency is close to the pinned–pinned frequency which, as revealed by previous studies, is important to corrugation formation.

In the study of rail roughness growth and rail corrugation formation, it is vital to know the tangential stress distribution in the contact patch and the slip velocity between the wheel and rail in the slip zone. In steady rolling contact problems, in which the contact force and the contact geometry are time-invariant, calculation methods have been well established [19], and analytical formulae are available for two-dimensional problems [11].

This paper presents a new effort on rail roughness growth, using a mixed frequency and time-domain approach. A wavenumber-based frequency-domain calculation method is used for the response of a periodically supported rail to a moving harmonic load [17,18], allowing dynamic wheel/rail forces to be calculated for single or multiple wheels moving over an initially smooth or rough track. This approach is more efficient than a full time-domain approach, but extends earlier work [13] by including the effect of forward motion explicitly. To evaluate the wear during the passage of the wheels, and hence a changed roughness for the rail, two methods of representing unsteady rolling contact are considered: a simple two-dimensional approach [20] and the approximate three-dimensional method using FASTSIM [21]. The former, similar to that adopted in Ref. [13], allows the nature of the effects to be investigated efficiently, whilst the latter provides more detail and allows validation of the simple approach. Both methods work effectively in the spatial domain allowing the spatial distribution of the roughness growth to be represented correctly. A great number of repetitions of such a process will demonstrate how rail roughness grows or corrugation forms. This paper concentrates on results of the modelling; further details of the models can be found in Ref. [20].

2. Wheel/track interaction

The dynamic interaction between the wheel and the track is calculated in the vertical direction. The track is assumed to be a periodic structure consisting of an infinite Timoshenko beam supported on hysteretically damped springs (representing the rail pads), masses (the sleepers) and another layer of hysteretically damped springs (the ballast). Such a Timoshenko beam model is known to provide a good representation of the vertical vibration of the rail up to about 2 kHz, above which the rail cross-section deformation should be taken into account [22]. One or more wheels, each represented by a mass, are connected to the track by their contact stiffness and are running along the track at constant speed c. Thus, although the model is based on the frequency domain, motion of the load and periodicity of the track are included in an efficient way [17,18]. For simplicity the roughness is also assumed to be periodic with the sleeper spacing, so that only wavelengths that are integer fractions of the sleeper spacing are included. This means, for example, that at around 50 mm wavelength which is the 12th harmonic the resolution of the wavelengths is about 4 mm. Even in the absence of roughness, a dynamic wheel/rail force is generated due to 'parametric excitation', that is, due to the time-varying stiffness of the track experienced by the wheels.

Details of the wheel/rail interaction model are given in Refs. [17,18]. The parameter values listed in Table 1 are used. Fig. 1 shows the vertical receptance of the rail for a static excitation, along with that of the contact spring and wheel mass for comparison. The dip at 250 Hz corresponds to the resonance of the sleepers on their supports (railpad and ballast) acting as a vibration absorber to the rail. The peak at about 500 Hz corresponds to the resonance of the rail on the railpad. The peak and dip at 1 kHz corresponds to the pinned–pinned vibration of the rail in which the bending wavelength in the rail equals twice the sleeper spacing. A second pinned–pinned mode, corresponding to a full bending wavelength between sleepers, occurs at 2.9 kHz. A wheel-on-track resonance will occur at about 50 Hz where the wheel and track receptances are approximately equal in magnitude and opposite in phase. When the wheel moves along the track, the displacement at the contact point is modified from this. In particular the peak at the pinned–pinned frequency is divided into two peaks [20].

The spectrum of wheel/rail force predicted for a smooth railhead (and wheel) is shown in Fig. 2(a). Note that, although shown as continuous spectra, the results in Fig. 2(a) consist only of components at the sleeper-passing frequency and its harmonics. The magnitude of the force fluctuations increases as speed increases.

The main component of the force fluctuation is at the sleeper passing frequency (67 Hz at 40 m/s), although the component at its second harmonic is as large for a speed of 60–80 m/s. At these speeds this component corresponds to a dip in the rail receptance at about 250 Hz, as seen in Fig. 1. A peak is also found at this frequency for 20 m/s, which is clearer due to the increased frequency resolution at the lower speed. A dip in the force spectrum occurs at around 500 Hz, corresponding to a peak in the rail receptance, and a peak in the force occurs at just above 1 kHz corresponding to the pinned–pinned frequency of the track. The contact force as a function of position within a sleeper bay can be reconstructed by using an inverse Fourier transform and is shown in Fig. 2(b).

Table 1
Parameters used for the vertical dynamics of the wheel/track system

Density of the rail	$7850\,kg/m^3$
Young's modulus of the rail	$2.1\times10^{11}\,N/m^2$
Shear modulus of the rail	$8.1\times10^{10}\,N/m^2$
Loss factor of the rail	0.01
Cross-sectional area of the rail	$7.69\times10^{-3}\,m^2$
Second moment of area of the rail cross-section	$3.055\times10^{-5}\,m^4$
Shear coefficient of the rail cross-section	0.4
Vertical rail pad stiffness	$3.5\times10^{8}\,N/m$
Rail pad loss factor	0.25
Mass of sleeper	162 kg
Sleeper spacing	0.6 m
Vertical ballast stiffness	$5\times10^{7}\,N/m$
Loss factor of ballast	1.0
Wheel/rail static load	$1\times10^{5}\,N$
Wheel mass	1350 kg
Wheel radius	0.575 m
Wheel/rail contact width ($2b$)	16 mm
Wheel/rail friction coefficient	0.3
Wear constant	$2.5\times10^{-9}\,kg/Nm$
Longitudinal creepage	0.001
Contact stiffness	$1.4\times10^{9}\,N/m$

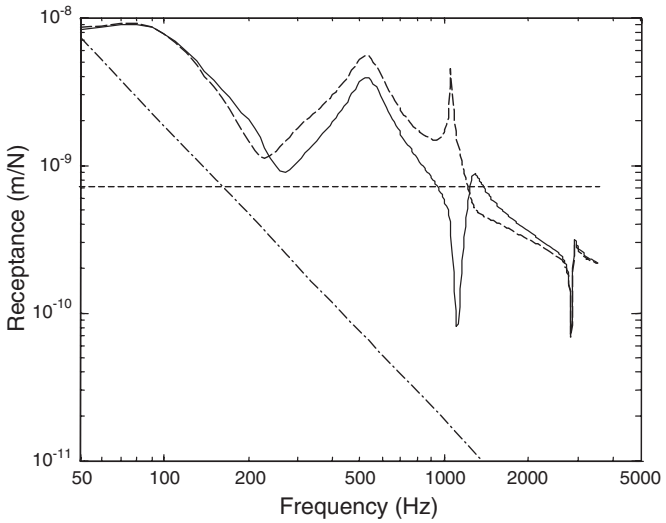

Fig. 1. Vertical receptances. ——, rail above sleeper; – – –, rail at mid-span; – · –, wheel; ……, contact spring.

3. Contact mechanics and wear

3.1. Two-dimensional contact model

The interaction model described in Section 2 produces a prediction of the vertical contact force which can be reconstructed into a time history, as shown in Fig. 2(b). At each position of the wheel along the rail, this force can be used to determine the vertical pressure distribution using the Hertz formulation [23]. In the two-

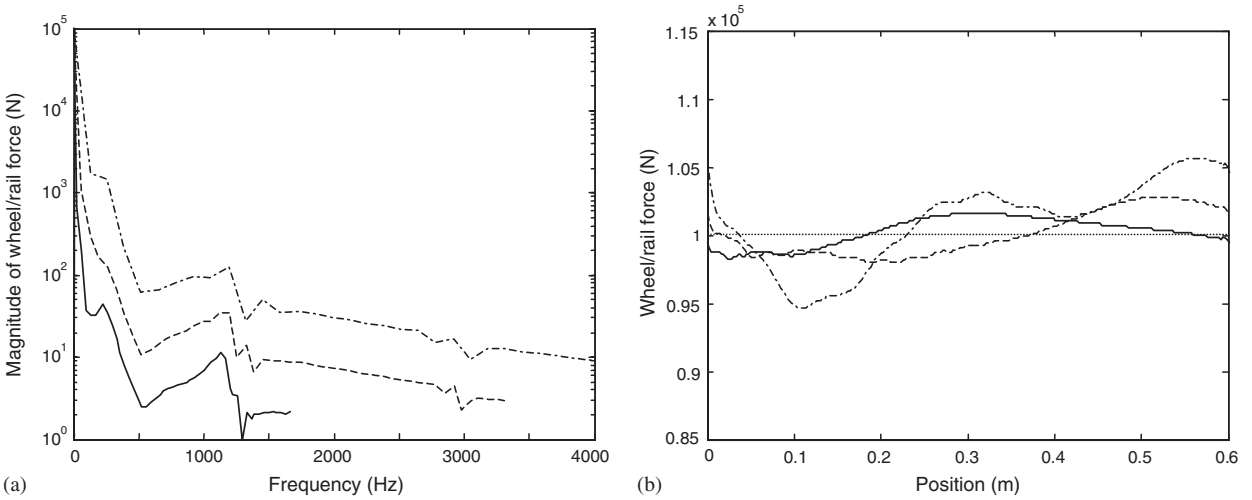

Fig. 2. Wheel/rail force predicted for the wheel moving at 20 m/s (——), 40 m/s (– – –) and 80 m/s (– · –) over the rail with a smooth railhead. (a) Spectrum, (b) position-history. Positions 0 and 0.6 m correspond to sleeper positions.

dimensional model used here, the contact is assumed to be between a cylinder representing the wheel and a flat rail surface, but with a constant contact patch width $2b$ set to 16 mm. Allowance is made for the curvature of the railhead in the longitudinal direction due to its roughness (if present). Although a linearised Hertz contact spring was used in the previous section in determining the interaction force time history, the model used in this section to determine the force distribution and hence the velocity and tangential stress is nonlinear.

A tangential force (in the longitudinal direction) is assumed to be generated from a constant value of longitudinal creepage, due for example to traction or braking. The creepage is the relative velocity between the wheel and rail normalised by the rolling velocity. In practice, the creepage varies with time, although much more slowly than the normal force, and could be calculated using a vehicle dynamics package. Here a constant value of 0.1% is assumed.

Within the contact patch an area near the leading edge is in adhesion (no relative motion) whereas an area near the trailing edge experiences sliding. To accommodate this sticking and sliding behaviour, tangential deformation occurs in the wheel and rail. According to Carter [11] there is a single sliding region and a single adhesion zone. The size of the sliding region increases as the creepage increases [19]. Relative motion only occurs in the sliding zone, where the tangential stress is equal to the normal pressure times the coefficient of friction. The model used is similar to Ref. [13]. Example results are shown in Fig. 3 for a sinusoidal roughness of wavelength 0.04 m and amplitude of 10 μm. The contact patch length and position of the stick-slip boundary can be seen to vary considerably during the cycle of roughness. Note that, although the relative velocity between wheel and rail is 0.1% of 40 m/s, i.e. 0.04 m/s, the local sliding velocity can be considerably larger than this near the trailing edge of the contact patch.

Wear is assumed to occur due to local relative motion. Various wear laws are available but here a simple frictional work model is used, as in Refs. [13,15]. Wear at a position is assumed to be proportional to the work done by the tangential stress at that position over the time during which the position experiences slip. The reduction in profile height $\Delta z(x)$ at a longitudinal position x on the rail due to one wheel passage is taken as

$$\Delta z(x) = \frac{1}{\rho}\int_{t_1}^{t_2} K|q(x,t)s(x,t)|\mathrm{d}t, \tag{1}$$

where ρ is the material density of the rail, q is the frictional stress, s is the relative velocity, $[t_1, t_2]$ is the time period during which the position x is in the nominal contact patch and K is a material-related constant determined by experiment. Here K is chosen to be 2.5×10^{-9} kg/Nm [15].

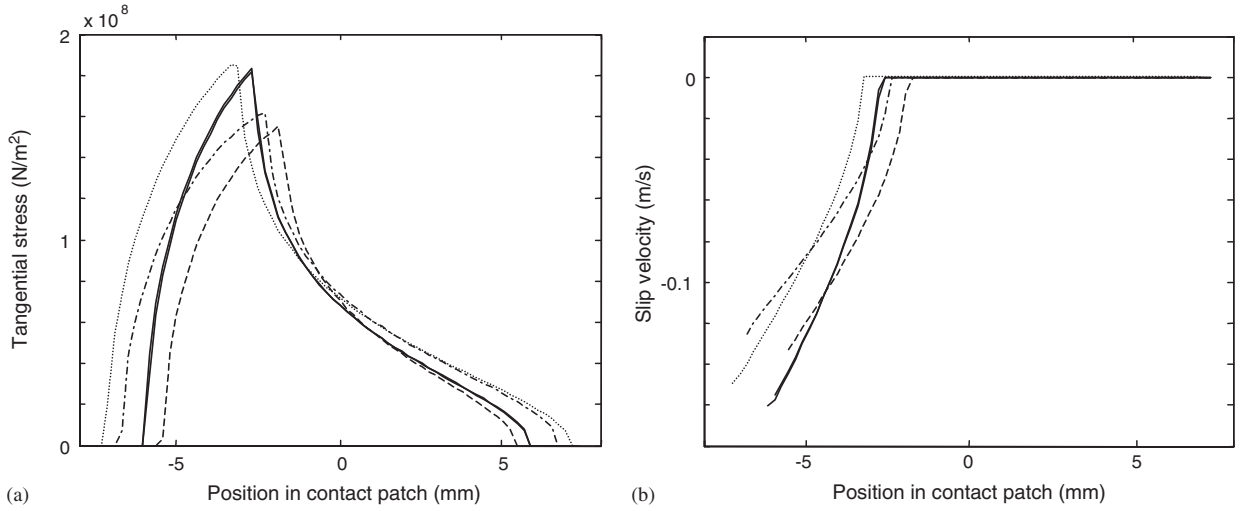

Fig. 3. (a) Tangential contact stress, (b) slip velocity, due to a single wheel moving at 40 m/s over a sinusoidal rail of wavelength 0.04 m and amplitude 10 μm. ——, $t = 0$; – – –, $t = 0.25$ ms ($x = 0.01$ m); – · –, $t = 0.5$ ms ($x = 0.02$ m); ……, $t = 0.75$ ms ($x = 0.03$ m); ——, $t = 1$ ms ($x = 0.04$ m).

3.2. FASTSIM model

The local wear rate in the contact patch can alternatively be calculated using a three-dimensional contact model. With the three-dimensional contact model, the effects of lateral creepages and spin on the roughness growth can be included. The various creepages can be obtained from a vehicle dynamics simulation. The lateral movement of the contact patch can also be included to predict the wear on the rail and wheel. However, here only a case equivalent to that considered above is treated.

For a roughness wavelength larger than 0.02 m, the normal pressure of the wheel/rail contact can be treated as Hertzian contact (elliptical contact patch). This assumption is valid if the contact patch is on the railhead without flange contact. In the present work, an elastic foundation model for the steady-state rolling contact is used. This is also referred to as the fast algorithm of the simplified theory of rolling contact (FASTSIM) by Kalker [21].

In FASTSIM, the elliptical contact patch is divided into a grid of elements. For a given normal force, the size of the contact ellipse can be determined according to the profiles of the wheel and rail. The calculation is performed on each slice parallel to the rolling direction, starting from the leading edge of the slice. The local slip velocity and tangential stress for each element will be obtained at the end of the iterative calculation.

The local wear rate is considered to be proportional to the friction work, the theory of which is well known. Johansson [24] presented a model to calculate the local wear rate using FASTSIM. The wear depth at each element after the wheel moves a distance equal to the length of the element is given by

$$\Delta Z = \frac{Kw}{\rho} = \frac{Kqs\,\Delta t}{\rho}, \tag{2}$$

where q and s are the local tangential stress and slip velocity in the longitudinal direction (if lateral slip is also allowed these become vector quantities), ρ is the density of the rail and Δt is time taken for the wheel to move the length of one element, which can be given by the length of the element divided by the wheel speed.

For a contact patch divided into a stick and a slip region, wear occurs only in the slip region as the slip velocity in the stick region is zero. When the normal force and creepages are varying, the slip and stick regions are not constant. This eventually leads to uneven wear on the railhead.

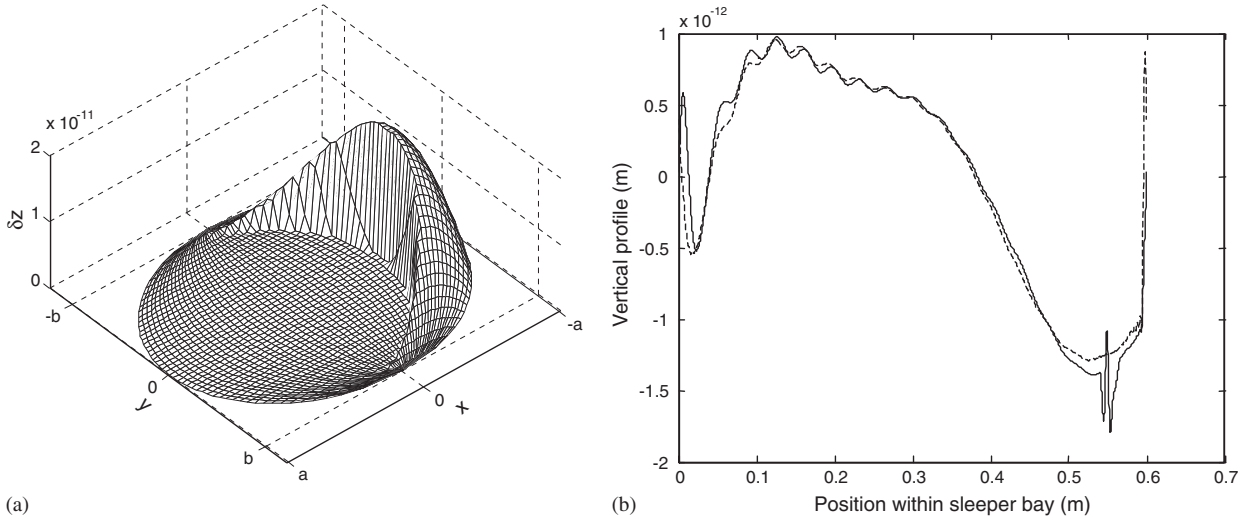

Fig. 4. (a) Local wear rate at the position of the maximum normal force. (b) Rail roughness obtained from a smooth rail for one wheel passage (40 m/s). ——, two-dimensional model; – – –, FASTSIM model.

3.3. Wear after one wheel passage

The wear after one wheel passage over a smooth rail for the distance between two sleepers is studied using the above two contact models. To compare with the results from the two-dimensional unsteady contact model, only longitudinal creepage is applied in the FASTSIM model. In the present case, the constant value of 0.1% for the longitudinal creepage is used. The dynamic normal force from Section 2 corresponding to a wheel speed of 40 m/s is used. A transverse rail radius of 1.55 m is used in the FASTSIM model. This gives elliptical contact patches approximately having the same area as the rectangular ones used in the two-dimensional model. The local wear rate at the position of the maximum force ($x = 0.55$ m) is presented in Fig. 4(a). It can be seen that zero wear occurs in the stick region. The local wear in the contact patch is symmetric about the x-axis as only longitudinal creepage is included.

The maximum wear occurs at the centre of the contact across the rail ($y = 0$). The accumulated wear on this line after one wheel passage is presented in Fig. 4(b), along with the result from the two-dimensional contact model. A good agreement is obtained between the two contact models for the present case, although the results from the FASTSIM model appear to be very sensitive to the choice of transverse rail radius.

4. Roughness growth

Roughness growth after a large number of wheel passages simulated using the two-dimensional contact model is presented in this section. The effects of train speed, rail pad stiffness and number of wheels (single or multiple) are studied.

4.1. Effect of speed

The development of roughness from an absolutely smooth rail is demonstrated in Fig. 5 for wheel speeds of 20 and 40 m/s. Each curve in these graphs represents the rail profile after a specified number of passages of a wheel. The number of wheel passages between each pair of adjacent profiles is 10,000. The mean wear of the rail has been removed from these results, so that values above 0 represent a smaller than average wear and values below 0 a greater than average wear. Starting from a smooth rail, roughness grows particularly at the wavelength of the sleeper spacing. Roughness at shorter wavelengths, corresponding to anti-resonances of the rail, develops simultaneously. For a wheel speed of 20 m/s, roughness at a wavelength of about 0.1 m is

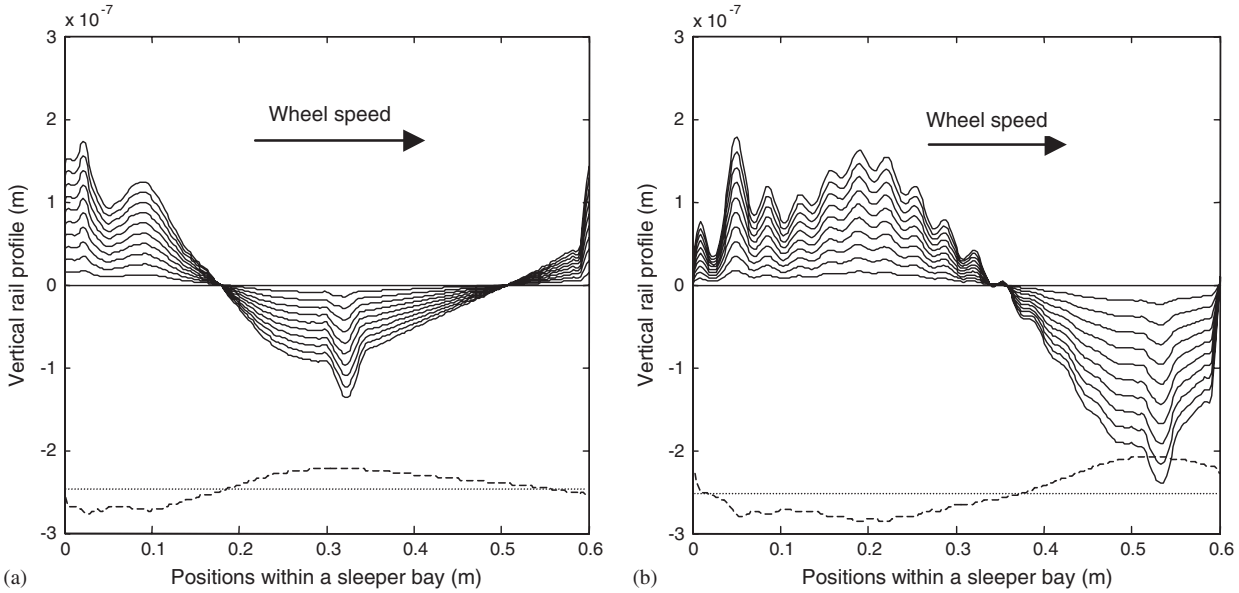

Fig. 5. Rail roughness evolution from a smooth rail. (a) Wheel speed 20 m/s. (b) Wheel speed 40 m/s. Each line represents the new profile after 10,000 wheel passages from the last. The variation of normal load from Fig. 2(b) is shown for comparison (- - -) not to the same scale.

developed just after a sleeper. This wavelength corresponds to the high stiffness of the rail at about 250 Hz. At 40 m/s, roughness of about 0.03–0.04 m is clearly seen in Fig. 5(b). At this speed this corresponds to the pinned–pinned frequency of just over 1 kHz.

The dynamic wheel/rail force from the parametric excitation is dominant over the dynamic wheel/rail force caused by the newly produced roughness [18] as the latter has still quite small amplitudes, of the order of 0.1 μm. It is noted from these figures that there are positions where the wear is always equal to the average wear in a sleeper bay and therefore the height of the roughness at these positions is zero after each passage of the wheel. The force is zero at these positions, as shown in Fig. 2(b). Comparison of Fig. 5 with Fig. 2(b) shows that a higher normal wheel/rail force corresponds to a greater removal of material from the railhead. The force is also reproduced in Fig. 5 for ease of comparison.

Fig. 6 shows the spectrum of the rail roughness produced by 100,000 wheel passages from a smooth rail for four wheels speed (20, 40, 60 and 80 m/s). It can be seen that roughness components at wavelengths of the sleeper spacing (wavenumber 10 rad/m), and a half and a third of this, increase with wheel speed and are dominant. These components are produced by the parametric excitation of the moving wheel. The overall spectrum slopes down towards higher wavenumbers, similar to measured roughness spectra [25].

The wavenumbers corresponding to the pinned–pinned frequencies are shown in Fig. 6 by arrows. At 20 m/s, the pinned–pinned frequency corresponds to a wavenumber of 330 rad/m (wavelength 19 mm) and does not appear as a peak. This is because, at this wheel speed, the corresponding wavelength is less than 0.02 m and the roughness component at this wavelength is filtered to a large extent by the wheel/rail contact patch. However at higher wheel speeds, short wavelength roughness corresponding to the pinned–pinned frequency becomes significant. Broad peaks are found in Fig. 6 at around 165 rad/m (38 mm wavelength) for 40 m/s and at 82 rad/m (76 mm) at 80 m/s. This is also seen in Fig. 5.

4.2. *Effect of pad stiffness*

The effect of the rail pad stiffness is demonstrated in Fig. 7. Fig. 7(a) shows the rail profile produced from a smooth rail after 100,000 passages by a single wheel moving at 40 m/s. The wavenumber spectrum of the profile is shown in Fig. 7(b). Two values of railpad stiffness, 3.5×10^8 and 0.7×10^8 N/m, are examined while

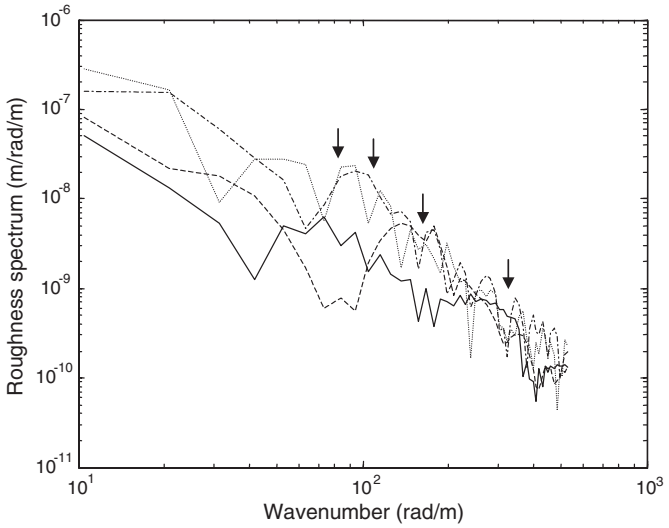

Fig. 6. Spectrum of the rail roughness produced by 100,000 wheel passages from a smooth rail. ——, wheel speed 20 m/s; – – –, wheel speed 40 m/s; – · –, wheel speed 60 m/s; ……, wheel speed 80 m/s. Arrows indicate the location of the pinned–pinned frequency at each speed, 330 rad/m at 20 m/s, 165 rad/m at 40 m/s, 110 rad/m at 60 m/s and 82 rad/m at 80 m/s.

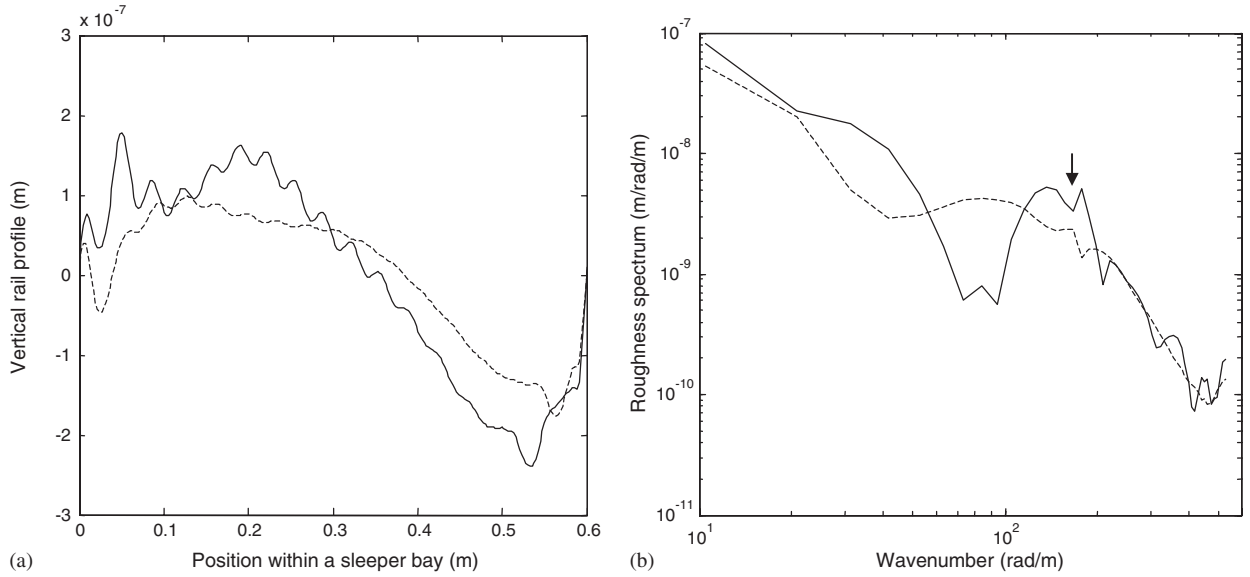

Fig. 7. (a) Rail roughness, (b) spectrum of rail roughness, produced by 100,000 wheel passages at 40 m/s from a smooth rail. ——, railpad stiffness 3.5×10^8 N/m; – – –, railpad stiffness 0.7×10^8 N/m. Arrow indicates the location of the pinned–pinned frequency at this speed, 165 rad/m.

other parameters are as listed in Table 1. It can be seen that, for most of the wavelengths, the softer rail pad reduces roughness growth, resulting in a lower overall roughness level. The prominent peak for the stiffer rail pad at a wavelength corresponding to the pinned–pinned frequency (about 0.33 m or a wavenumber of 19 rad/m) is reduced by the reduction in rail pad stiffness and becomes broader and smoother, indicating that corrugation at that wavelength is far less evident. In other words, soft rail pads can prevent corrugation formation, although broad-band roughness is still formed.

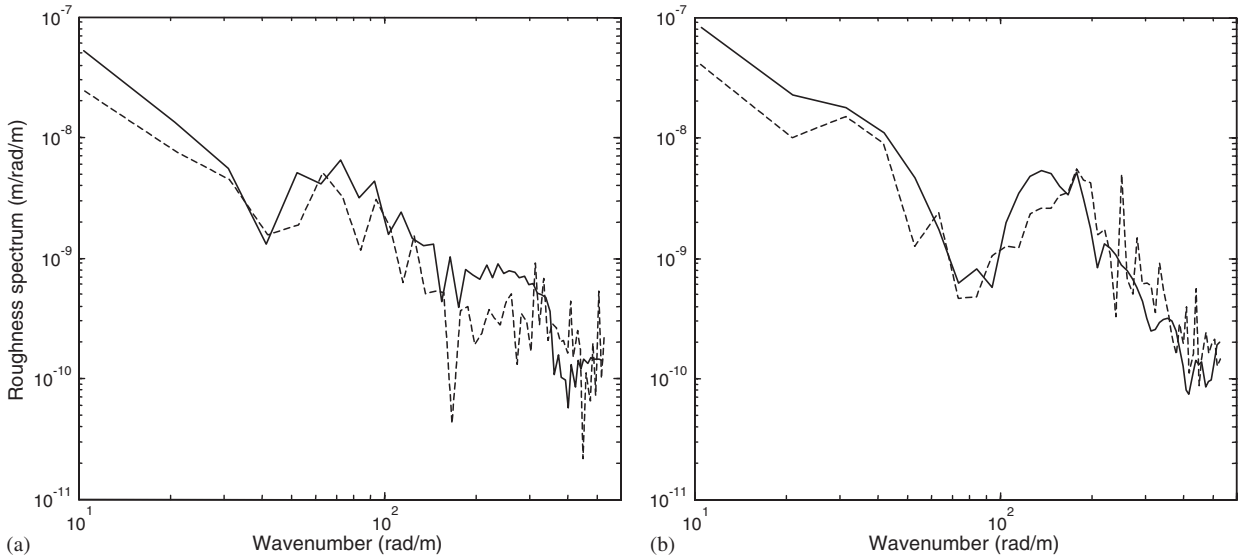

Fig. 8. Spectra of the rail roughness produced by 100,000 wheel passages from a smooth rail. ——, single wheel model; – – –, multiple (four) wheel model (one passage of the two bogies equals four wheel passages). (a) Wheel speed 20 m/s, (b) wheel speed 40 m/s.

4.3. Effect of multiple wheels

The above results have been presented for a single wheel. In other words, for each passage there is only a single wheel moving along the track, excluding the effects from adjacent wheels in a bogie. As shown in Refs. [12,18], the normal wheel/rail force at a wheel can be affected by other wheels, especially at excitation frequencies at which interference occurs between the wheels. Fig. 8 shows the effects of the presence of multiple wheels on roughness growth. Here four driving wheels from two bogies in a British Class 87 electric locomotive are present for each passage. The bogie wheelbase is 3.3 m and the distance between the bogie centres is 10 m. The main effect is that the multiple wheel model shows reduced roughness growth compared with a single wheel model at most wavenumbers. This may be explained by the fact that maximum wear occurs at different positions for different wheels. Compared with the single wheel model, the multiple wheel model produces extra dips and peaks. These peaks and dips are caused by the interferences between the wheels, and the corresponding wavelengths are determined by, among other things, the separations of the wheels.

5. Conclusions

An investigation into rail roughness growth is presented which overcomes some of the shortcomings found in previous studies. Using the wavenumber-based calculation method for the response of a periodically supported rail to a moving static or harmonic load, dynamic wheel/rail forces are calculated for multiple wheels moving over an initially smooth or rough rail. Removal of material from the rail rolling surface is evaluated using a simple energy based wear model and two-dimensional unsteady contact mechanics theory. A large number of repetitions of such a process demonstrate how rail roughness grows and corrugation forms.

Results from the roughness growth prediction model show that parametric excitation has a significant contribution to the initiation of rail roughness. The amount of roughness growth depends strongly on excitation frequency, with maximum growth found to occur near the pinned–pinned frequency. A low railpad stiffness is shown to reduce roughness growth as found in previous studies, although broad-band roughness still develops. The multiple-wheel model predicts less roughness growth than the single-wheel model, showing that these effects should be included in a quantitative model of roughness growth.

The rolling contact between the wheel and rail is also modelled using an approximate three-dimensional model, FASTSIM. The wear after one wheel passage predicted using the two contact models is compared.

This provides some justification for using the simpler model, although more detailed results are obtained from the FASTSIM approach.

In real situations, wheel/rail contact is subject to time-varying longitudinal, lateral and spin creepages. To extend the current work beyond a single assumed creepage value of 0.1%, further studies of roughness initiation and growth at different creepage amplitudes are required using the three-dimensional contact model.

Acknowledgements

This work was supported by the EPSRC and Rail Research UK under project A3: Railway noise: curve squeal, roughness growth, friction and wear.

References

[1] D.J. Thompson, Theory of generation of wheel/rail rolling noise, in: V.V. Krylov (Ed.), *Noise and Vibration from High-Speed Trains*, Thomas Telford, London, 2001.
[2] D.J. Thompson, B. Hemsworth, N. Vincent, Experimental validation of the TWINS prediction program for rolling noise, part I: description of the model and method, *Journal of Sound and Vibration* 193 (1996) 123–135.
[3] N. Vincent, P. Bouvet, D.J. Thompson, P.E. Gautier, Theoretical optimisation of track components to reduce rolling noise, *Journal of Sound and Vibration* 193 (1996) 161–171.
[4] H. Ilias, The influence of railpad stiffness on wheel/track interaction and corrugation growth, *Journal of Sound and Vibration* 227 (1999) 935–948.
[5] S.L. Grassie, J. Kalousek, Rail corrugation: characteristics, causes and treatments, *Proceedings of the Institute of Mechanical Engineers, part F: Journal of Rail and Rapid Transit* 207 (1993) 57–68.
[6] S. Müller, A linear wheel-track model to predict instability and short pitch corrugation, *Journal of Sound and Vibration* 227 (1999) 899–913.
[7] A. Valdivia, Interaction Between High-frequency Wheel–Rail Dynamics and Irregular Rail Wear—a Linear Model, Ph.D. Dissertation, TU, Berlin, 1987.
[8] K. Hempelmann, K. Knothe, An extended linear model for the prediction of short-pitch corrugation, *Wear* 191 (1996) 161–169.
[9] C.O. Frederick, A rail corrugation theory, in: *Proceedings of the Second Conference on the Contact Mechanics and Wear of Rail/Wheel Systems*, 1986.
[10] J.B. Nielsen, Evolution of rail corrugation predicted with a non-linear wear model, *Journal of Sound and Vibration* 227 (1999) 915–933.
[11] F.W. Carter, On the action of a locomotive driving wheel, *Proceedings of the Royal Society of London, A* 112 (1926) 151–157.
[12] T.X. Wu, D.J. Thompson, Behaviour of the normal contact force under multiple wheel/rail interaction, *Vehicle System Dynamics* 37 (2002) 157–174.
[13] T.X. Wu, D.J. Thompson, An investigation into rail corrugation due to micro-slip under multiple wheel/rail interactions, *Wear* 258 (2005) 1115–1125.
[14] A. Igeland, Dynamic Train/Track Interaction: Simulation of Railhead Corrugation Growth Under a Moving Bogie Using Mathematical Models Combined with Full-scale Measurements. Ph.D. Thesis, Chalmers University of Technology, 1997.
[15] J.C.O. Nielsen, Numerical prediction of rail roughness growth on tangent tracks, *Journal of Sound and Vibration* 267 (2003) 537–548.
[16] C. Andersson, A. Johansson, Prediction of rail corrugation generated by three-dimensional wheel–rail interaction, *Wear* 257 (2004) 423–434.
[17] X. Sheng, C.J.C. Jones, D.J. Thompson, Responses of infinite periodic structures to moving or stationary harmonic loads, *Journal of Sound and Vibration* 282 (2005) 125–149.
[18] X. Sheng, D.J. Thompson, C.J.C. Jones, Interactions between a moving wheel and a periodically supported rail. *Proceedings of IOA Spring Conference*, Southampton, March 2004, pp. 80–91.
[19] J.J. Kalker, *Three-Dimensional Elastic Bodies in Rolling Contact*, Kluwer Academic Publishers, Dordrecht, 1990.
[20] X. Sheng, D.J. Thompson, C.J.C. Jones, Modelling rail roughness growth on tangent tracks, Institute of Sound and Vibration Research Technical Memorandum 929, 2004.
[21] J.J. Kalker, A fast algorithm for the simplified theory of rolling contact, *Vehicle System Dynamics* 11 (1982) 1–13.
[22] T.X. Wu, D.J. Thompson, A double Timoshenko beam model for vertical vibration analysis of railway track at high frequencies, *Journal of Sound and Vibration* 224 (1999) 329–348.
[23] K.L. Johnson, *Contact Mechanics*, Cambridge University Press, Cambridge, 1987.
[24] A. Johansson, Mathematical models for simulation of wheel–rail rolling contact and for prediction of wear—survey of models for calculation of creep forces, spin moments and wear depths, Department of Applied Mechanics, Chalmers University of Technology, Gothenburg, Sweden, 2003, ISSN 1651-0208.
[25] P.C. Dings, M.G. Dittrich, Roughness on Dutch railway wheels and rails, *Journal of Sound and Vibration* 193 (1996) 103–112.